Integral imaging with extended depth of field

Manuel Martínez-Corral*, Raúl Martínez-Cuenca, Genaro Saavedra, and Bahram Javidi+
Department of Optics, University of Valencia, E46100 Burjassot, Spain
+Electrical and Computer Engineering Dept, University of Connecticut, Storrs, CT 06269-1157

ABSTRACT

One of the main drawbacks on integral imaging systems is their limited depth of field. With the current state of sensor technology such limitation is imposed by the pixilated structure of cell detectors. So, depth of field only can be optimized by proper selection of system parameters. However, nowadays sensor technology experiments a fast development. As a result of it, it is sure that in a close future the number of pixels per elemental image will be high enough to not influence the system resolution. In this not-too-far context, new ideas should be applied to improve the depth of field of integral imaging systems. Here we propose a new method to significantly extend the depth of field. The technique is based on the combined benefits of a proper amplitude modulation of the microlenses, and the application of deconvolution tools.

Key words: Three-dimensional image acquisition, Multiple imaging, Resolution, Depth of field.

1. INTRODUCTION

Currently, much visual information is presented to users through computer monitors, TV screens, or even through cellular-phone or PDA screens. The displayed images can have entertainment or information values, or even be aimed at the diffusion of research results [1]. The information society increasingly demands the display of not only plane images but also of three-dimensional (3D) images, or even movies [2-5], with continuous perspective information. Although the search for optimum 3D imaging and display techniques has been the subject of research from much more than for a century [6], it has been in the last several years when technology is approaching the level required for realization of 3D imaging systems. The so-called integral imaging (InI), which is a 3D imaging technique specially suited for the above requirements, works with incoherent light, and provides with auto-stereoscopic images without the help of any special glasses. In an InI system, an array of microlenses generates, onto a sensor such as a CCD, a collection of plane elemental images. Each elemental image has a different perspective of the 3D object. Therefore, the CCD records a set of the object projections. In the reconstruction stage, the recorded images are displayed by an optical device, such as a LCD monitor, placed in front of another microlens array. This setup provides the observer with a reconstructed 3D image with full parallax. InI was first proposed by Lippmann [7], and some relevant work was done in the meantime [8-12]. The interest in InI has been resurrected recently because of its application to 3D TV and display [13].

Since its rebirth, InI has overcome many of its challenges. Specifically, it is remarkable that a simple technique for the pseudoscopic to orthoscopic conversion was developed [14]. Some methods were proposed to overcome the limits in lateral resolution imposed by the CCD [15-17], or by the microlens array [18,19]. Other challenge satisfactorily faced is of the limitation in viewing area [22]. Apart from this engineering work, some purely theoretical work has been also performed to characterize the response in resolution of InI systems [23,24], or the viewing parameters in the display stage [25,26].

At present 3D InI systems still face some problems. One issue is the limited depth of field (DOF). In a typical scene objects exist at different depth positions. Since only a single plane is used to capture the images, it is not possible for all objects to be in focus. Then blurred images of out-of-focus objects, or part of objects, are obtained. Although the DOF of InI systems is influenced by many parameters (related with both the capture and the display systems), it is apparent that to display a clear integral image of an axially elongated 3D object it is essential to capture sharp 2D elemental images of it. For this reason, the bottleneck of the DOF in InI is the limited depth of focus of the microlens array used in the pickup stage. In systems with low-resolution sensors one can overcome this problem by reducing the numerical aperture (NA) of the lenses [27]. In the past few years, some new alternative techniques have been proposed to improve the depth of field of integral imaging systems. These methods are based on the synthesis of real and virtual image fields [28], or on the use of lenses with non-uniform focal lengths and aperture sizes [29,30].

* manuel.martinez@uv.es; phone +34 96354 4718; fax +34 96354 4715; www.uv.es/imaging3

Three-Dimensional TV, Video, and Display IV
edited by Bahram Javidi, Fumio Okano, Jung-Young Son
Proc. of SPIE Vol. 6016, 601602, (2005)· 0277-786X/05/$15 · doi: 10.1117/12.626790

In this paper we propose a new method for producing a significant enlargement of the DOF of InI pickup system. This enlargement is not accompanied by a deterioration of spatial resolution. The method, whose main feature is its simplicity, is based on an adequate binary modulation of the microlenses amplitude transmittance [31]. To present our technique we start by carrying out a theoretical analysis of the pickup stage of integral imaging systems, in terms of the scalar diffraction theory. This analysis explicitly takes into account the fact that the object is a surface object. This assumption allows us to develop a set of equations, which constitutes a strict description of the diffractive behavior of the pickup of an integral imaging system. This analysis shows us that, conversely to what is generally assumed, integral imaging systems are not linear and shift invariant, and therefore it is not valid, *stricto senso*, to define neither a point spread function (PSF) nor an optical transfer function (OTF). In a second step, we design an adequate amplitude modulator, which should be applied to any element of the microlens array. Later, we take advantage of deconvolution concept to propose a technique for important enlargement of the DOF [32]. We have performed numerical simulations with computer-synthesized objects, to show that the DOF of focus is significantly improved.

2. PRINCIPLES OF INTEGRAL IMAGING

Integral photography was proposed by Lipmann in 1908 [7]. In his scheme, a photography of a self-luminous 3D scene is taken through a pinhole array (see Fig.1). This pickup setup provides with a set of micro-images, named hereafter to as the elemental images, each having information of a different perspective of the object. In the display stage properly processed film is placed in front of the same pinhole array and back illuminated so that each elemental image acts as a spatially incoherent object. As shown in the figure allows the reconstruction of a real, but depth reversed image of the 3D scene.

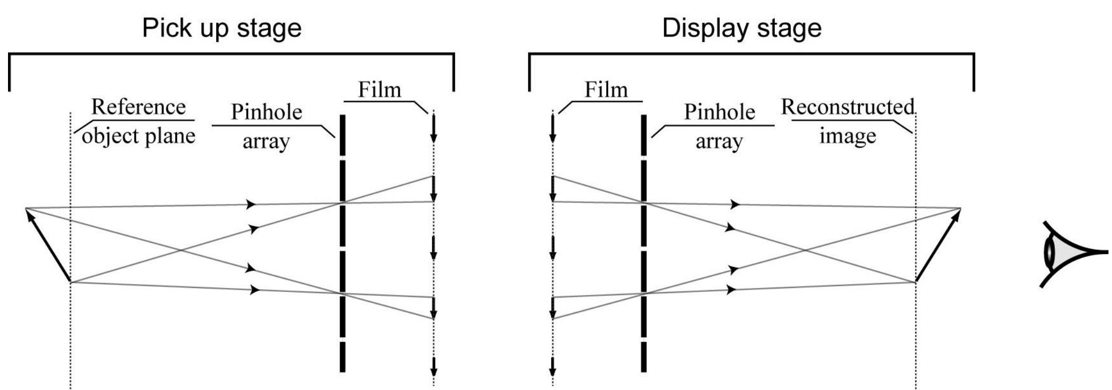

Figure 1.- Scheme of the integral photography method proposed by Lipmann.

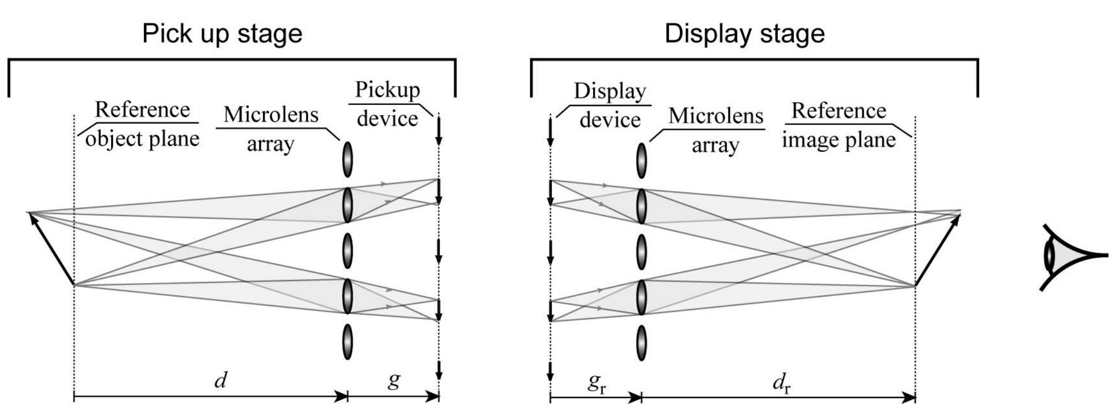

Figure 2.- Scheme of an integral imaging system

The major drawback of the scheme proposed by Lipmann is its extremely poor light efficiency, the second problem is that the film processing inherent to a photographic process is very slow and does not match the current requirements of 3D imaging. A solution of these problems is to substitute the pinhole array by a microlens array and the photographic film by an electronic sensor like a CCD. As shown in Fig. 2, now the elemental images are formed in the image plane of the microlenses. However, now an important problem appears: the limitation in DOF. Due to the imaging properties of the lenses, now only one plane of the object space is in focus. Then light proceeding from other planes does not focus onto the CCD. The same problem happens in the display stage. Only points within the object plane are reconstructed sharply. Other parts of the 3D scene are increasingly blurred. Besides, this blurring effect is more significant when the pixilation of the CCD (or the LCD in the display stage) is taken into account. Consequently, this new realization of the integral imaging process gives rise to much more luminous reconstructed images, but with low resolution even in case of the in-focus plane.

Other remarkable feature of InI systems is the facetted form of the reconstructed integral images. When the observer places the eye in front of the lenslets array and looks through it to see the reconstructed image, he/she sees a different portion of the image through any different lenslet. Such image portions are the elemental fields of view (FOVs) provided by any microlens. Depending on the system geometry, the elemental FOVs, may overlap or may not, giving rise, in some cases, to reconstructed images divided in multiple facets. Such multi-facet structure can degrade the quality of the observed image, because it breaks the continuity of its visual aspect. In Fig. 3 we have schematize the observation of the image, for the case of real pseudoscopic reconstruction. The image is reconstructed by superposition of projected elemental images, each one with different perspective. The observer is placed at a distance D from the microlens array. Take into account that the distance from the observer to the reconstructed image, $D-d_{\mathrm{r}}$, must be larger than the nearest distance of distinct vision which, for the case of an adult observer, is about $250\,mm$. As heuristically shown in Fig. 3, the observer's full FOV is composed by a collection of elemental FOVs arranged in a rectangular grid. In Fig. 4 we show an example of the facetted structure of the image. To minimize this detrimental effect, a proper selection of the system parameter should be done [26].

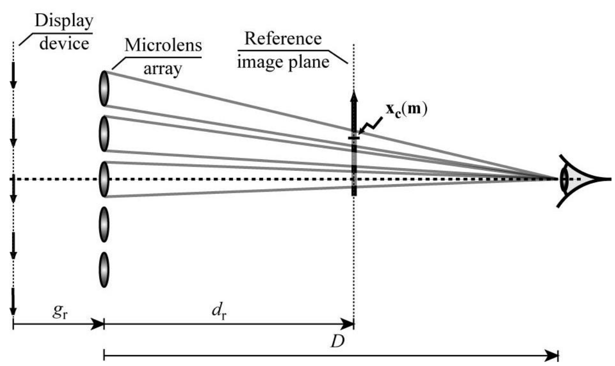

Figure 3.- Observation of reconstructed real image. The observed image consists on a rectangular grid of elemental FOVs. Each elemental FOV is observed through a different microlens.

Other problem that has deserved many research efforts but still has not found, as the best of our knowledge, an optimum solution is the pseudoscopic-to-orthoscopic (PO) conversion. As it is well known, in their standard configuration InI systems provide the observer with real, pseudoscopic images, that is, with a 3D reconstruction of the object that is reversed in depth (see Fig.2). A very smart and simple scheme was suggested by Okano and co-workers [13]. They proposed to capture the elemental images with the standard pickup architecture. Then, each elemental image is rotated by 180º around the center of the elemental cell. Taking into account the pixilated structure of the elemental images, this operation only implies a simple pixel mapping. As we show in Fig. 5, when these rotated elemental images are displayed at a distance $g_v=g-2f^2/(d-f)$, a virtual, undistorted orthoscopic image is obtained at a distance $d_v=d-2f$ from the lenslets array. Although in this scheme there is not degradation of the image due to the introduction of additional elements or stages, it still has the drawback that the reconstructed image is virtual.

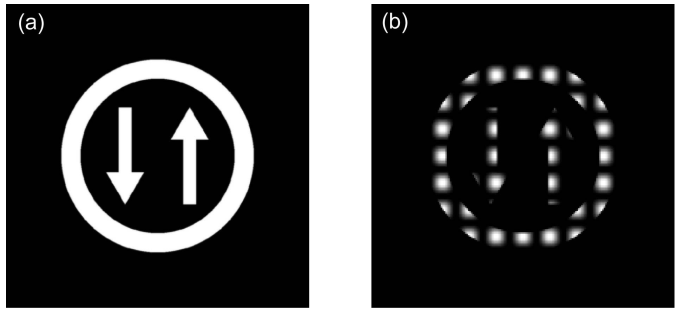

Figure 4.- (a) Synthetic object used for the numerical simulation, (b) Reconstructed image as seen by the observed when set at $D = 900\, mm$ and a microlenses filling factor of 0.5.

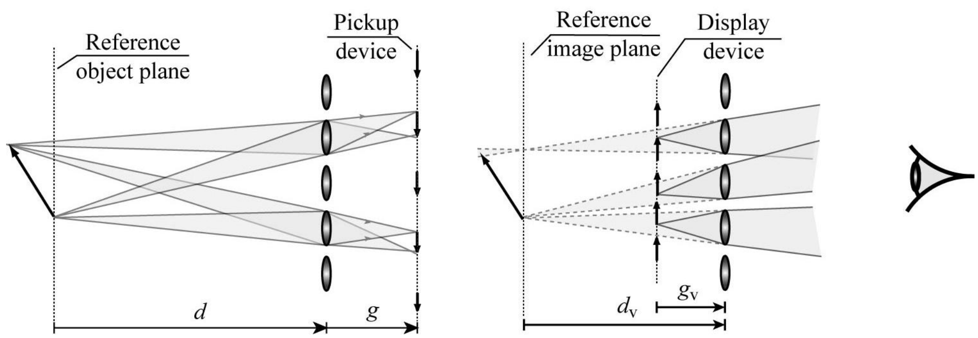

Figure 5. Schematic drawing of the orthoscopic, virtual reconstruction. In the display stage the elemental images are rotated by 180º around the center of the cell.

3. THEORETICAL ANALYSIS OF THE CAPTURE STAGE

We start by describing the capture stage from the point of view of diffraction theory. Let us remark that since the microlens arrays generally used in typical InI experiments are of low numerical aperture ($NA \approx 0.1$), the analysis can be accurately performed within the frame of the paraxial scalar diffraction theory. In Fig. 6 we show a scheme of the capture setup. Spatial coordinates are denoted $\mathbf{x} = (x, y)$ and z for directions transverse and parallel to the system main optical axis. We consider a surface object under spatially incoherent illumination. For simplicity we assume quasi-monochromatic illumination with mean wavelength λ. Light emitted by the surface object is collected by the microlens array to form a collection of 2D elemental aerial images. The images are formed in the so-called aerial pickup plane, which is set at a distance g from the microlens array. The reference and the aerial pickup plane are conjugated through the microlenses, so that distances a and g are related by the lens law $1/a+1/g-1/f=0$. Any elemental image has a different perspective of the surface object. In our scheme a relay system, composed by a field lens and a camera lens, is used to image the aerial images into the pickup device (usually a CCD camera). The lateral magnification of the relay system is adjusted so that the size of the elemental-images collection array matches the CCD.

The intensity distribution of incoherent light scattered by the object can be represented by the real and positive function

$$O(\mathbf{x}, z) = R(\mathbf{x})\delta(z - f(\mathbf{x})) \ , \qquad (1)$$

where function $R(\mathbf{x})$ accounts for the object intensity reflectivity, whereas $f(\mathbf{x}) - z = 0$ is the function that describes the surface.

We consider now the light scattered at an arbitrary point $(\mathbf{x}, z)$ of the surface object. It is straightforward, by application in cascade of paraxial scalar diffraction equations, to find that the intensity at a given point $\mathbf{x'} = (x', y')$ of the aerial pickup plane is given by

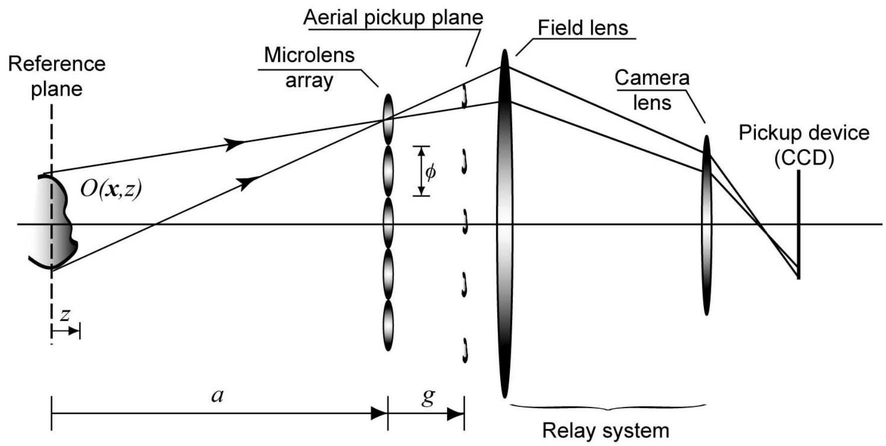

Figure 6. Scheme, not to scale, of the capture setup of a 3D InI system. Object points out of reference plane produce blurred images in the CCD. In the relay system the field lens collects the rays from the outer microlenses; the camera lens projects the images onto the CCD.

$$H_\lambda(\mathbf{x}';\mathbf{x},z)=\left|\sum_{\mathbf{m}}\exp\left\{i\frac{\pi}{\lambda(a-z)}|\mathbf{m}p-\mathbf{x}|^2\right\}\int \mathsf{P}_z(\mathbf{x_o})\exp\left\{-i2\pi\mathbf{x_o}\frac{\mathbf{x}'+[M_z(\mathbf{m}p-\mathbf{x})-\mathbf{m}p]}{\lambda g}\right\}d^2\mathbf{x_o}\right|^2, \tag{2}$$

where $\mathbf{m}=(m,n)$ accounts for the microlenses indexes in the (x,y) directions, and p stands for the constant pitch of the microlens array. In Eq. (2) $M_z=-g/(a-z)$ is a magnification factor that depends on the depth coordinate z. The so-called generalized pupil function is:

$$\mathsf{P}_z(\mathbf{x_o})=p(\mathbf{x_o})\exp\left\{i\frac{\pi}{\lambda}\left(\frac{1}{a-z}-\frac{1}{a}\right)|\mathbf{x_o}|^2\right\}. \tag{3}$$

This function accounts for the microlenses pupil function, $p(\mathbf{x_o})$, together with the phase modulation due to defocus errors. It is important to remark that, in principle, the matter of interest of our research is not the intensity distribution at the aerial pickup plane, but the distribution at the pickup-device plane. Note however that since such a distribution is simply a uniformly scaled version of the one in Eq. (2), it is correct to base our study on such an equation.

Assuming non significant overlapping between the elemental diffraction spots provided by the different microlenses, Eq. (2) can be rewritten in quite good approximation as the 2D convolution between the, properly scaled, 2D Fourier transform of $\mathsf{P}_z(\mathbf{x_o})$ and a sampling function, that is

$$H_\lambda(\mathbf{x}';\mathbf{x},z)=\left|\tilde{\mathsf{P}}_z\left(\frac{\mathbf{x}'}{\lambda g}\right)\right|^2\otimes\sum_{\mathbf{m}}\delta\{\mathbf{x}'-[\mathbf{m}p(1-M_z)+M_z\mathbf{x}]\}\ . \tag{4}$$

Let us consider now the overall light proceeding from the surface object. In this case the intensity distribution in the pickup plane is obtained as a weighted superposition of the diffraction spots provided by any point of the surface object, namely

$$I_\lambda(\mathbf{x}')=\int R(\mathbf{x})\delta(z-f(\mathbf{x}))H_\lambda(\mathbf{x}';\mathbf{x},z)\,d^2\mathbf{x}\,dz=\int R(\mathbf{x})H_\lambda(\mathbf{x}';\mathbf{x},z=f(\mathbf{x}))\,d^2\mathbf{x} \tag{5}$$

Note that function $H_\lambda(\bullet)$ explicitly depends on $\mathbf{x}'-M_z\mathbf{x}$, that is:

$$H_\lambda(\mathbf{x}';\mathbf{x},z)=H_\lambda(\mathbf{x}'-M_z\mathbf{x};0,z)\equiv H_\lambda(\mathbf{x}'-M_z\mathbf{x};z). \tag{6}$$

Then, Eq. (5) can be rewritten as

$$I_\lambda(\mathbf{x}') = \int R(\mathbf{x}) H_\lambda(\mathbf{x}' - M_z\mathbf{x}; z = f(\mathbf{x})) d^2\mathbf{x} \,. \tag{7}$$

Although Eq. (7) seems to represent a 2D convolution, it does not. This is because function $\mathsf{P}_z(\mathbf{x_o})$ has a strong dependence on the axial position of the corresponding surface points. In other words, function $H_\lambda(\bullet)$ is different for different values of z. Besides, factor M_z also depends on z, and therefore parts of the object at different depth are magnified in different way. Consequently, the impulse response is different at any depth. This fact implies that, the pickup system is not linear and shift invariant. Therefore, neither the PSF nor the OTF could be rigorously defined.

As seen above, the acquired image is composed by an array of elemental images of the surface object, each one obtained from a different viewpoint. Let us now focus our attention into the elemental image produced by one of the microlenses, for example the one in the center of the microlens array (this selection does not subtract any generality from our study). The intensity distribution of such an elemental image is given by

$$I_\lambda^{o}(\mathbf{x}') = \int R(\mathbf{x}) H_\lambda^{o}(\mathbf{x}' - M_z\mathbf{x}; z) d^2\mathbf{x} \,, \tag{8}$$

where

$$H_\lambda^{o}(\mathbf{x}'; z) = \left| \tilde{\mathsf{P}}_z\left(\frac{\mathbf{x}'}{\lambda g}\right) \right|^2 \,. \tag{9}$$

We assume that the pupil of each microlens is a circle with diameter ϕ. In such a case, it is convenient to express Eq. (9) in cylindrical coordinates as follows

$$H_\lambda^{o}(r, z) = \left| \int_0^{\phi/2} p(r_o) \exp\left\{ i \frac{\pi}{\lambda} \frac{z}{a(a-z)} r_o^2 \right\} J_o\left(2\pi \frac{r\, r_o}{\lambda g} \right) r_o \, dr_o \right|^2 \,. \tag{10}$$

4. THE INFLUENCE OF THE DETECTOR PIXEL SIZE

Let us revisit at this point the concepts of lateral resolution and DOF. The resolution of an imaging system evaluates its capacity for producing sharp images of the finest features of the object, when it is in focus. In case of diffraction-limited imaging systems, resolution is usually evaluated in terms of the Rayleigh criterion. According to it, the resolution of the pickup system under study is determined by the radius of the first zero ring of the Airy disk, $H_\lambda^{o}(\mathbf{x}; z)$. Note that the central lobe contains 84% of the energy in the Airy disk. On the other hand, The DOF of an imaging system is the distance by which the object may be axially shifted before an unacceptable blur is produced. In diffraction-limited imaging systems, the DOF is usually evaluated in terms of the so-called Rayleigh range: the axial distance from the in-focus plane to the point that produces an spot whose radius has increased by a factor $2^{1/2}$. The evaluation of the radii of the spots produced by out-of-focus points ($z \neq 0$) is not as simple as in the in-focus case. This is because as z increases the spot spreads and neither a central lobe nor zero ring are recognized. In this case we define the defocused-spot diameter as the one of a circle that encircles 84% of the overall pattern energy. In mathematical terms such diameter, $D(z)$, is the one which solves the equation

$$\int_0^{D/2} H_\lambda^{O}(\mathbf{x}, z) d\mathbf{x} = 0.84 \int_0^{\infty} H_\lambda^{O}(\mathbf{x}, z) d\mathbf{x} \,. \tag{11}$$

In Fig. 7(b) we represent, with t hick line, the defocused-spot diameter for different values of distance z. We conclude, from the figure, that if only the limits imposed by diffraction are considered, the resolution limit of the pickup system under study is of is of 3.33 μm, measured in the aerial pickup plane, and the DOF is, for positive values of z, of +8.5 mm.

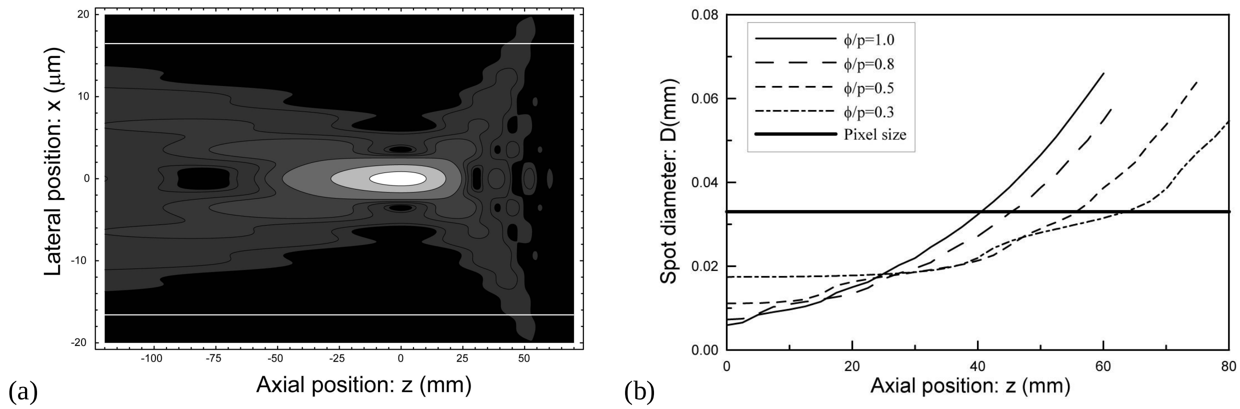

Figure 7. (a) Grey-scale representation of Eq. 10. Any cross-sections correspond to the spot produced by an object point at a depth z. White lines delimit the back-projected pixel size. The effect of defocus is much more appreciable for positive values of z; (b) Spot diameter for different values of the fill factor. The black thick line is used to mark the back-projected pixel size.

To appreciate the influence of pixilation on the lateral resolution at any depth position of the object, we assumed that the CCD has 1024x768 square pixels and the array has 34x25 microlenses. Therefore each elemental image has 30x30 pixels. In Fig. 7(a), we have drawn a pair of horizontal lines separated by a distance that equals the back projection of the pixel size onto the aerial pickup plane. When the intensity spot is smaller than the (back projected) pixel size, the resolution limit is imposed by the pixilated structure of the CCD. On the contrary, when the intensity spot is bigger than the pixel size, the resolution limit is imposed by diffraction. In Fig. 7(b) we have plotted a horizontal thick line that corresponds to the back-projected pixel size. From this figure, some important properties of the captured elemental images can be deduced: (a) The resolution limit for objects at $z=0$ is determined by the CCD pixel size. This limit is much higher than the one imposed by diffraction; (b) For objects in a large range of axial positions z, the resolution limit is still imposed by the CCD. Therefore this limit is the same as for objects at $z=0$; (c) For objects beyond the above range, the resolution is imposed by the spot diameter, which rapidly increases as z increases. (d) The range of axial positions in which the resolution limit does not change, defines now the DOF of the capture setup of an InI system.

Then we can conclude that, contrarily to what is commonly assumed, in a large rage of depth positions the lateral reso-lution of the capture setup is determined not by diffraction but by the CCD. This fact provides us with one additional degree of freedom in the design of the optimum pickup. Specifically, one can safely increase the DOF by use of techniques that in diffraction-limited systems would deteriorate the lateral resolution at $z=0$. In this sense, one can decrease the lenslets fill factor, defined as the quotient between the diameter of the microlenses, ϕ, and the pitch, p. It is known that decreasing the lenslets fill factor, produces the increase of the spot diameter at $z=0$, but a significant reduction for larger values of z. Reducing the fill factor does not affect to the lateral resolution at z=0 (which is determined by the CCD), but importantly increases the DOF. In Fig. 7(b), we have represented the evolution of the spot diameter for different values of the fill factor. All the cases represented have the same lateral resolution at low values for z. However,

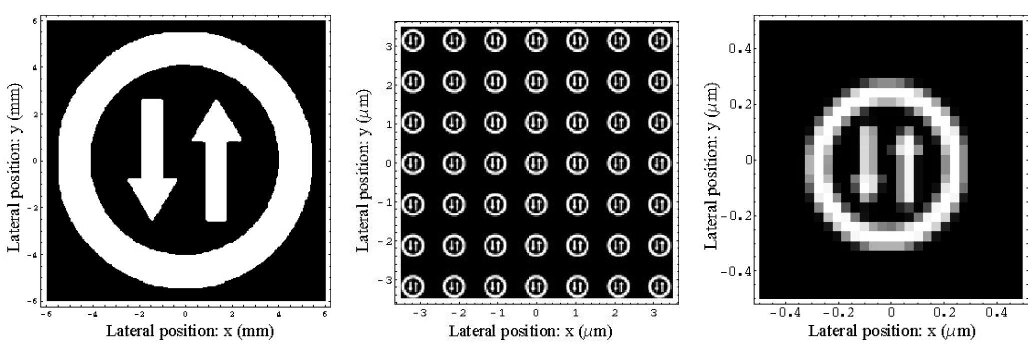

Figure 8. (a) Synthetic object; (b) 2D elemental images captured from 49 views; (c) Enlarged view of the central image. The object was placed at $z=0$ and the fill factor was set at $\phi/p=1.0$

for example, the DOF obtained with ϕ/p=0.5 is 40% longer than the one obtained with ϕ/p=1.0. At z=54 mm the resolution limit obtained with ϕ/p=0.5 is half of the one obtained with a fill factor of 1.

To further illustrate our proposal, we have performed a numerical imaging experiment with a computer-generated synthetic object, see Fig 8(a). In the first step, we have calculated the elemental images assuming that the object was placed at z=0 and the fill factor is ϕ/p=1.0. The images captured from 49 different views are shown in Fig. 8(b). In Fig. 8(c) we show an enlarged image of the central element **m**=(0,0). Next, in Fig. 9, we show the elemental images obtained with the fill factor ϕ/p=0.5. There are no differences in resolution between this image and the one obtained with ϕ/p=1.0.

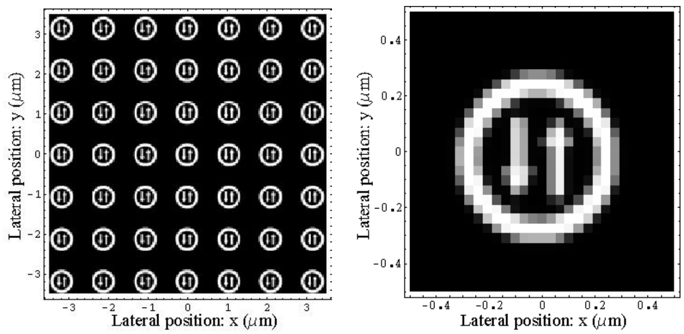

Figure 9. (a) 2D elemental images of the object captured from 49 different views; (b) Enlarged view of the central image. The object was placed at z=0 and the fill factor was set at ϕ/p=0.5.

In Fig. 10 we show the of the central elemental image obtained when the synthetic object is axially displaced to z=67.5 mm. Note that the magnification factor M_z increases with z. It is apparent that for large values of z the resolution obtained with ϕ/p=0.5 is much better than the resolution obtained with of ϕ/p=1.0.

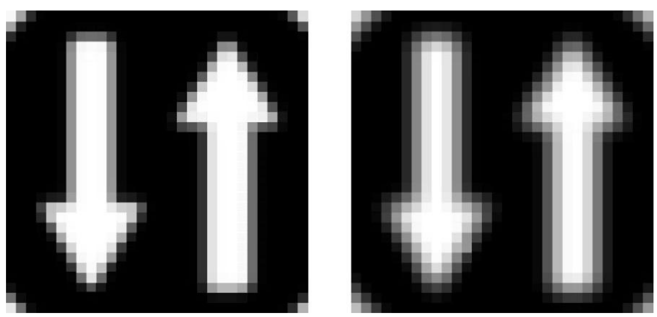

Figure 10. Central elemental image as the object is displaced from z=0 to z=67.5 mm. Left-hand image corresponds to ϕ/p=0.5. Right-hand one to ϕ/p=1.0.

5. THE BINARY AMPLITUDE MODULATION

In Fig. 11(a) we have represented some cross-sections of Eq. (10). The parameters for the calculation were: ϕ=2.0 mm, f=5.0 mm, λ=0.5 μm, and a=100 mm. Note that, due to the low value for the lens NA, the axial extent of H_λ^o is much higher than the lateral extent. In the section z=0 we can recognize the Airy disk pattern, whose extent determines the lateral resolution of the system. We find that in this case the resolution limit, as defined by Rayleigh, is of 1.61 μm, if measured in the pickup plane, or of 30.6 μm if evaluated in the reference object plane. The DOF is usually evaluated by means of the so-called Rayleigh range, which is defined as the extent of the axial interval in which $H_\lambda^o(0;z)$ is higher than $\sqrt{2}/2$ times its maximum value [33]. In this case, the Rayleigh range is $-3.3\,mm < z < 3.1\,mm$. Let us remark that, as we see in the following section, the pixel size of the capture device is a factor that strongly influences the DOF and the resolution. However, in our calculations at this stage we have considered that the pixels are sufficiently fine.

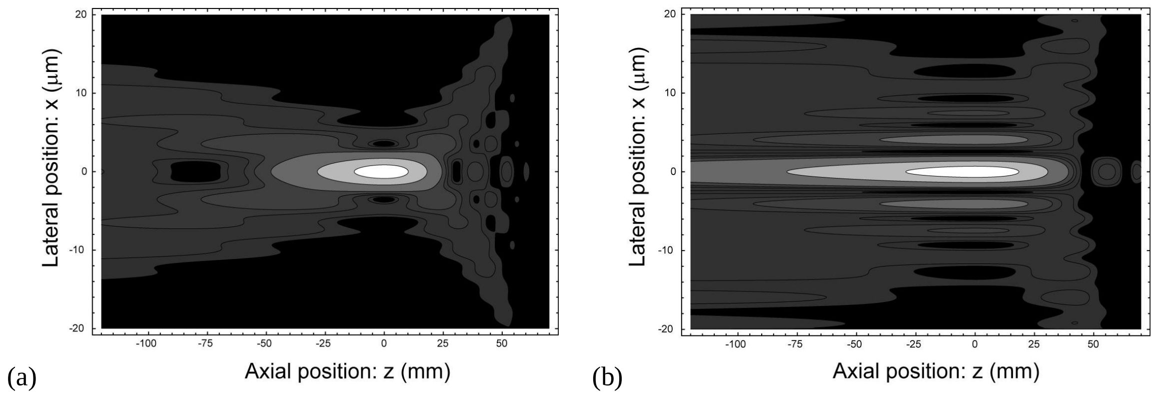

Figure 11. Meridian section of function $H_{\lambda}^{\mathbf{0}}(\mathbf{x},z)$ corresponding to: (a) the non-modulated lenses; and (b) the amplitude-modulated lenses. The filters consist in an opaque circular mask of diameter $\delta\phi$ (with $\delta = 1/\sqrt{2}$) centered just behind each microlens.

To illustrate the limitations in DOF of an integral imaging system, we have performed a numerical experiment in which we obtain the elemental images of a computer-synthesized object. Since the aim of the experiment is to appreciate the improvement in DOF, we have selected as the object the Snellen **E** tumbling chart, which is usually used to grade resolution and defocus errors in visual optics. In the experiment the **E** patterns are positioned side by side and are longitudinally located at z_1=-10.0 *mm*, z_2=-5.0 *mm*, z_3=+4.6 *mm*, z_4=+8.3 *mm*, respectively, as depicted in Fig. 12. Note that the axial positions are not symmetric about the reference plane, but corresponds to the same amount of defocus as defined in terms of the well-known defocus coefficient $\omega_{20} = z\phi^2 / 2\lambda a(a-z)$ [34]. The elemental images were calculated according to Eq. (7). In Fig. 13(a) we show the central element **m**=(0,0). It is clear from the figure that the images of the **E** patterns in z_1 and z_4 are highly blurred. Let us remark that, since the imaging system is not telecentric [35], the images corresponding to planes with the same modulus of ω_{20} but different sign are different. This is due to the different scale of defocused images. Due to this effect, the elemental image of the **E** patterns located at z_1 is much more blurred than the elemental image corresponding to the **E** pattern at z_4. It is noticeable that in the case of the pattern at z_1 one can hardly distinguish the original orientation of the **E** in the elemental image.

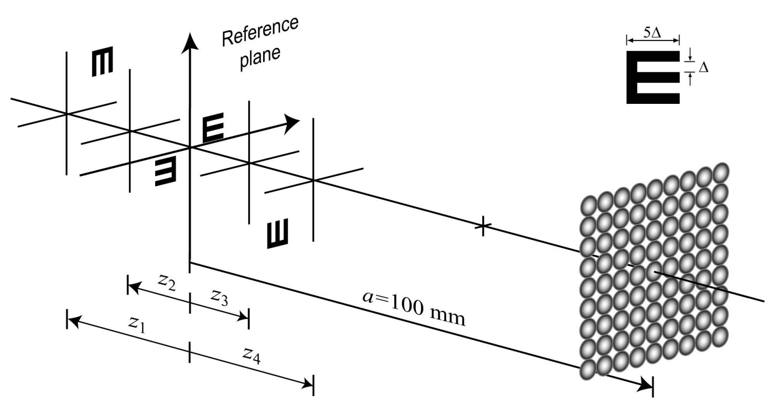

Figure 12. Scheme, not to scale, of the integral imaging numerical experiment. The size of the legs of the charts used in our experiments is $\Delta = 51\mu m$, which is about two times the Rayleigh resolution limit.

The problem of the limited DOF can be overcome by use of amplitude-modulation techniques. Specifically we propose the use of binary amplitude modulators. Such kind of modulators have been successfully applied to improve the performance of other 3D imaging techniques such as confocal microscopy [36] or multiphoton scanning microscopy [37]. The technique consists in obscuring the central part of each microlens. Such an obscuration allows the secondary Huygens wavelets proceeding from the outer part of the lenses to interfere constructively in an enlarged axial range.

Then by simply placing an opaque circular mask of diameter D=δϕ (with 0<δ<1) just behind each microlens, one can increase the focal depth of the microlens array. It is known that the higher the value of the obscuration ratio δ, the broader the axial intensity spot. In an ideal case one could obtain infinite depth of focus by approaching the value of δ to the unity. However, such a situation is not convenient from an experimental point of view, because the higher the value of δ the smaller the light efficiency of the system. On the other hand, if one works with only the outermost part of the lenses, the optical aberrations of the system dramatically increase. For these reasons, we propose to use the binary modulator of obscuration ratio $\delta=\sqrt{2}/2$. This modulator has a light efficiency of 50%, and doubles the depth of focus of the system.

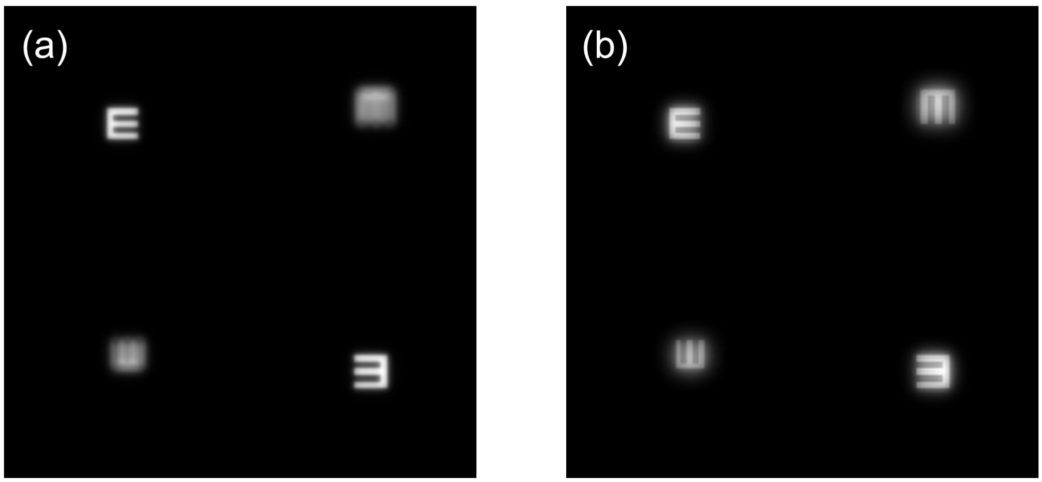

Figure 13. 2D central elemental images captured with the microlens array. We do not show the whole field of view, but only a portion of $0.4\,\mathrm{mm}\times0.4\,\mathrm{mm}$ centered at the corresponding optical axis. (a) Image obtained with the non-modulated microlenses; (b) Image obtained with the amplitude-modulated microlenses.

In Fig. 11(b), we have represented some cross-sections of Eq. (10), for the case of amplitude modulation with obscuration ratio $\delta=\sqrt{2}/2$. In this case, the Rayleigh resolution limit is 22.3 μm (as evaluated in the reference plane), whereas the DOF is -6.8 mm< z <+6.0 mm. If we compare these results with the ones obtained with the non-modulated setup (see Fig. 11(a)) we find that the DOF has been doubled, and the 2D density of resolved points has been increased by a factor of 1.85. Also in this case we have performed the numerical experiment with the same Snellen **E** tumbling chart as in the previous section. The central elemental image, **m**=(0,0), is shown in Fig. 13(b). One observes the noticeable improvement in DOF provided by the amplitude modulation phase elements method. Note on the other hand, that the images of objects at z_2 and z_3 are slightly more blurred than the ones obtained with the non-modulated architecture. This fact seems to contradict the statement that the binary modulation improves the lateral resolution, as defined by Rayleigh, for objects placed at any depth z. Take into account, however, that the Rayleigh resolution limit is defined for point objects, and therefore it does not hold in case of more elaborated objects. In such a case, the use of binary amplitude modulation improves lateral resolution in a very large range of depth positions, but produces a slight worsening for low values of depth coordinate z.

Summarizing, we have found that the use of binary amplitude-modulated microlens arrays permits an important improvement of the DOF of InI systems. This is because the amplitude-modulation technique allows the impulse response to change much more slowly with axial displacements of the object. Thus we see that the impulse responses remain practically invariant over a wide range of values of z. In other words, the use of amplitude-modulated microlenses permits to consider, in quite good approximation that the system is LSI over a wide range of axial distances and therefore, to define an effective PSF, which will be named as $H_{eff}(\mathbf{x})$. So in this context deconvolution tools can be applied over a wide range of axial object positions.

6. DECONVOLUTION TOOLS: THE WIENER FILTERING

In real 2D image acquisition tasks, the recorded signal, $i(\mathbf{x})$, depends not only on the convolution between the input signal and the PSF, but also on the noise signal. In mathematical terms,

$$i(\mathbf{x}) = s(\mathbf{x}) \otimes h(\mathbf{x}) + n(\mathbf{x}) \tag{12}$$

In this equation, $s(\mathbf{x})$ represents the input signal, $h(\mathbf{x})$ stands for the PSF, and $n(\mathbf{x})$ accounts for any type of additive noise. To recover the input signal from the output, one should perform a deconvolution operation. There are two general types of deconvolution methods: linear and non-linear methods. The latter are more accurate, but they are all iterative methods. Since real-time processing is required in InI for a high number of elemental images, a low-time-consuming non-iterative method is mandatory.

The optimal linear method for the signal recovery problem is the Wiener filtering [38]. The Wiener filter is given by

$$W(\mathbf{u}) = \frac{\tilde{h}^*(\mathbf{u})\ |\tilde{s}(\mathbf{u})|^2}{|\tilde{h}(\mathbf{u})|^2 |\tilde{s}(\mathbf{u})|^2 + |\tilde{n}(\mathbf{u})|^2} \tag{13}$$

where $\tilde{f}(\mathbf{u})$ stands for the Fourier transform of $f(\mathbf{x})$ and * denotes complex conjugation. Since $s(\mathbf{x})$, and therefore $\tilde{s}(\mathbf{u})$, is unknown, the filter cannot be used to recover the image. However, if we assume that we deal with white noise and a constant spectrum for the object, this expression can be approximated to

$$W(\mathbf{u}) = \frac{\tilde{h}^*(\mathbf{u})}{|\tilde{h}(\mathbf{u})|^2 + c\varphi^2} \tag{14}$$

where φ^2 can be understood as the noise-to-signal ratio in the frequency domain (NSRf) and the parameter $c \in \Re^+$ controls the strength of the filtering. This filter is applied to the spectrum of the recorded signal

$$\tilde{\sigma}(\mathbf{u}) = \tilde{i}(\mathbf{u})\ W(\mathbf{u}) \tag{15}$$

and the recovery function $\sigma(\mathbf{x})$ is finally obtained by performing an inverse 2D Fourier transform of Eq. (15).

In the previous section we showed that by the use of the amplitude-modulated microlenses the InI. systems can be considered LSI in a neighborhood of the in-focus plane. Then Wiener filtering can be applied to recover the elemental images by using the effective PSF. After a thorough study of the method, we selected as $H_{eff}(\mathbf{x})$ the impulse response provided by an object point placed at z_{mid}=+23 *mm*. This PSF can be easily obtained by experimental measurement of the defocused spot produced by one microlens. The deconvolution procedure is performed by using this measured PSF [39]. Strictly speaking, only objects placed at this distance will be exactly recovered. Objects placed at other axial positions will be recovered quite approximately.

To illustrate the utility of our method, we have performed a numerical experiment. In the simulation we used the pickup architecture shown in Fig. 14, were we consider that the microlenses are amplitude modulated. Since the aim of the numerical experiment is the recovery of an arbitrary object, we selected the spoke target for the simulations. Note that the target contains information of a very wide range of spatial frequencies. To avoid under-sampling problems in the central zone of the target due to the pixelated structure of digitized images, we used a modified version of it in which the central zone was removed. Then we have applied the above-described deconvolution procedure to the acquired elemental images. The recovered elemental images are shown in Fig. 15 were, to make the experiment more visual, we have simulated the display process. In our calculations we assume an observer that is placed at a distance D=300 mm from the microlens array and sees the reconstructed virtual orthoscopic image. We have calculated the observed image for three different lateral positions of the observer, so that we can visualize the changes in perspective produced when the observer's eye is displaced parallel to the microlens array. This figure, together with Fig. 5, shows that the proposed method provides a very efficient extension of DOF in InI.

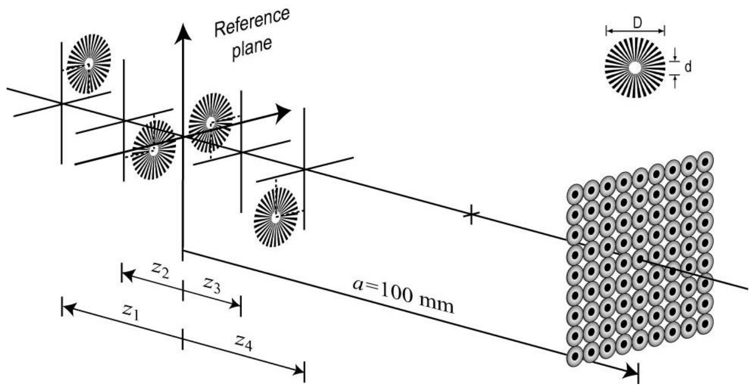

Fig. 14. Scheme, not to scale, of the integral imaging numerical experiment. The inner and outer diameters of the spoke target used in our experiments were $d = 0.4$ mm and $D = 2.0$ mm.

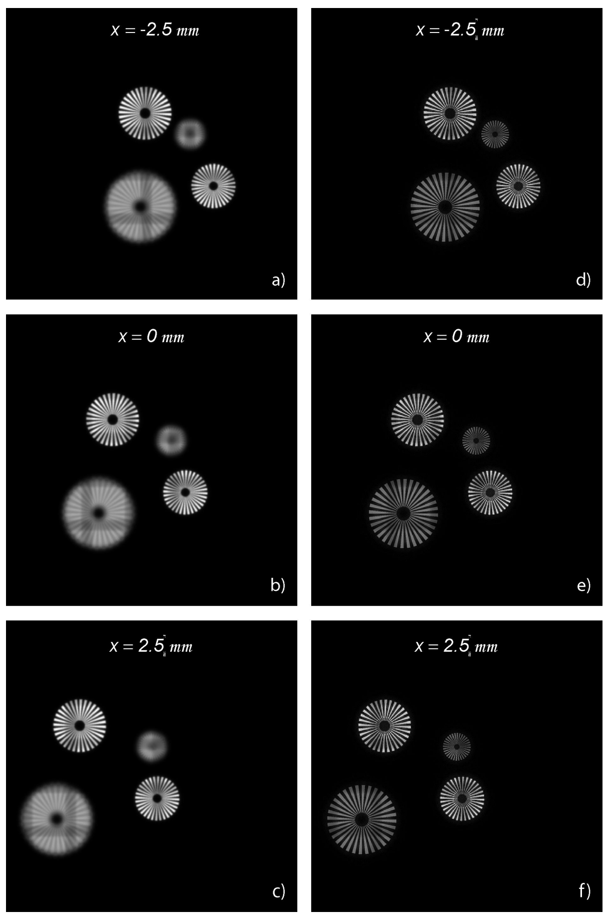

Fig. 15. Reconstructed image as seen by the observer from three different lateral positions. The series of pictures correspond to: (a-c) The case in which neither the amplitude modulation nor the Wiener filtering were applied in capture procedure; (d-f) The case in which both techniques were applied.

6. CONCLUSIONS

We have proposed a new method to significantly extend the depth of field for 3D image pick-up in InI. In our two-step method we first proposed the insertion of a binary amplitude modulator, which alters the system's impulse response to have certain invariance over a wide range of axial distances. This fact allowed us to define an effective PSF which, otherwise, could not be defined. In the second step we adapted the Wiener deconvolution procedure to the InI sensor. After applying the deconvolution tool, we have obtained elemental images in which the DOF has been spectacularly extended. We have illustrated our method with a numerical experiment in which we have recovered the high-frequency information of a synthetic object even for the most defocused planes. The proposed method has broad applications in 3DTV, 3D display, and 3D recognition.

ACKNOWLEDGEMENTS

This work has been funded in part by the Plan Nacional I+D+I (grant DPI2003-4698), Ministerio de Ciencia y Tecnología, Spain. R. Martínez-Cuenca gratefully acknowledges financial support from the University of Valencia (Grant Cinc Segles). We also acknowledge the funding from the Generalitat Valenciana, Spain (grant grupos03/227).

REFERENCES

1. J.-S. Jang and B. Javidi, "Three-dimensional integral imaging of micro-objects," Opt. Lett. **29**, 1230-1232 (2004).
2. H. Liao, M. Iwahara, N. Hata and T. Dohi, "High-quality integral videography using multiprojector," Opt. Express **12**, 1067-1076 (2004).
3. S. A. Benton, ed., Selected Papers on Three-Dimensional Displays (SPIE Optical Engineering Press, Bellingham, WA, 2001).
4. D. H. McMahon and H. J. Caulfield, "A technique for producing wide-angle holographic displays," Appl. Opt. **9**, 91-96 (1970).
5. P. Ambs, L. Bigue, R. Binet, J. Colineau, J.-C. Lehureau, and J.-P. Huignard, "Image reconstruction using electro-optic holography," *Proc. of the 16th Annual Meeting of the IEEE Lasers and Electro-Optics Society, LEOS 2003*, vol. 1 (IEEE, Piscataway, NJ, 2003) pp. 172-173
6. T. Okoshi, "Three-dimensional displays," Proc. IEEE **68**, 548-564 (1980).
7. M. G. Lippmann, "Epreuves reversibles donnant la sensation du relief," J. Phys. (Paris) **7**, 821-825 (1908).
8. H. E. Ives, "Optical properties of a Lippmann lenticuled sheet," J. Opt. Soc. Am. **21**, 171-176 (1931).
9. C. B. Burckhardt, "Optimum parameters and resolution limitation of integral photography," J. Opt. Soc. Am. **58**, 71-76 (1968).
10. T. Okoshi, "Optimum design and depth resolution of lens-shet and projection type three-dimensional displays," Appl. Opt. **10**, 2284-2291 (1971).
11. N. Davies, M. McCormick and L. Yang, "Three-dimensional imaging systems: a new development," Appl. Opt. **27**, 4520-4528 (1988).
12. N. Davies, M. McCormick and M. Brewin, "Design and analysis of an image transfer system usig microlens array," Opt. Eng. **33**, 3624-3633 (1994).
13. F. Okano, H. Hoshino, J. Arai and I. Yayuma, "Real time pickup method for a three-dimensional image based on integral photography," Appl. Opt. **36**, 1598-1603 (1997).
14. J. Arai, F. Okano, H. Hoshino and I. Yuyama, "Gradient-index lens-array method based on real-time integral photography for three-dimensional images," Appl. Opt. **37**, 2034-2045 (1998).
15. L. Erdmann and K. J. Gabriel, "High resolution digital photography by use of a scanning microlens array," Appl. Opt. **40**, 5592-5599 (2001).
16. S. Kishk and B. Javidi, "Improved resolution 3D object sensing and recognition using time multiplexed computational integral imaging," Opt. Express **11**, 3528-3541 (2003).

17. A. Stern and B. Javidi, “Three-dimensional image sensing and reconstruction with time-division multiplexed computational integral imaging”, Appl. Opt. **42**, 7036-7042 (2003).
18. J.-S. Jang and B. Javidi, "Three-dimensional synthetic aperture integral imaging," Opt. Lett. **27**, 1144-1146 (2002).
19. J.-S. Jang and B. Javidi, "Improved viewing resolution of three-dimensional integral imaging by use of nonstationary micro-optics," Opt. Lett. **27**, 324-326 (2002).
20. J.-S. Jang and B. Javidi, "Large depth-of-focus time-multiplexed three-dimensional integral imaging by use of lenslets with nonuniform focal lengths and aperture sizes," Opt. Lett. **28**, 1924-1926 (2003).
21. M. Martínez-Corral, B. Javidi, R. Martínez-Cuenca, and G. Saavedra, “Integral imaging with improved depth of field by use of amplitude modulated microlens array”, Appl. Opt. (in press).
22. H. Choi, S.-W. Min, S. Jung, J.-H. Park and B. Lee, "Multiple-viewing-zone integral imaging using dynamic barrier array for three-dimensional displays," Opt. Express **11**, 927-932 (2003).
23. J. Arai, H. Hoshino, M. Okui and F. Okano, "Effects on the resolution characteristics of integral photography," J. Opt. Soc. Am. **20**, 996-1004 (2003).
24. H. Hoshino, F. Okano, H. Isono and I. Yuyama, "Analysis of resolution limitation of integral photography," J. Opt. Soc. Am. A **15**, 2059-2065 (1998).
25. J.-H. Park, S.-W. Min, S. Jung and B. Lee, "Analysis of viewing parameters for two display methods based on integral photography," Appl. Opt. **40**, 5217-5232 (2001).
26. M. Martínez-Corral, B. Javidi, R. Martínez-Cuenca and G. Saavedra, "Multifacet structure of observed reconstructed integral images," J. Opt. Soc. Am. A **22**, 597-603 (2005).
27. R. Martínez-Cuenca, G. Saavedra, M. Martínez-Corral and B. Javidi, "Enhanced depth of field integral imaging with sensor resolution constraints," Opt. Express **12**, 5237-5242 (2004).
28. J.-S. Jang, F. Jin, and B. Javidi, "Three-dimensional integral imaging with large depth of focus by use of real and virtual image fields," Opt. Lett. **28**, 1421-1423 (2003).
29. B. Lee, S.-W. Min, S. Jung, and J.-H. Park, “Computer generated dynamic three-dimensional display using integral photography adopting Fesnel lensens,” Proc. SPIE **4471**, 9-17 (2001).
30. J.-S. Jang and B. Javidi, "Large depth-of-focus time-multiplexed three-dimensional integral imaging by use of lenslets with nonuniform focal lengths and aperture sizes," Opt. Lett. **28**, 1924-1926 (2003).
31. M. Martínez-Corral, B. Javidi, R. Martínez-Cuenca and G. Saavedra, "Integral imaging with improved depth of field by use of amplitude-modulated microlens array," Appl. Opt. **45**, 5806-5813 (2004).
32. R. Martínez-Cuenca, G. Saavedra, M. Martínez-Corral and B. Javidi, "Extended depth-of-field 3D display and visualization by combination of amplitude-modulated micro lenses and deconvolution tools," IEEE J. Disp. Technol. (in press).
33. A. E. Siegman, *Lasers* (Univ. Science, Saulito, CA 1986).
34. A. Stokseth, "Properties of a Defocused Optical System," J. Opt. Soc. Am. **59**, 1314-1321 (1969).
35. C. J. Zapata-Rodríguez, P. Andrés, M. Martínez-Corral, and L. Muñoz-Escrivá, "Gaussian imaging transformation for the paraxial Debye formulation of the focal region in a low-Fresnel-number optical system," J. Opt. Soc. Am. A **17**, 1185-1191 (2000).
36. M. Martínez-Corral, C. Ibáñez-López, G. Saavedra, and M. T. Caballero, “Axial gain resolution in optical sectioning fluorescence microscopy by shaded-ring filters,” Opt. Express **11**, 1740-1745 (2003).
37. C. Ibáñez-López, G. Saavedra, G. Boyer and M. Martínez-Corral, "Quasi-isotropic 3-D resolution in two-photon scanning microscopy," Opt. Express **12**, 6168-6174 (2005).
38. C. W. Helstrom, “Image restoration by the method of least squares,” J. Opt. Soc. Am., **57**, 297-303 (1967).
39. X. Lai, Zhiping Lin, E. S. Ward and R. J. Ober, “Noise suppression of point spread functions and its influence on deconvolution of three-dimensional fluorescence microscopy image sets,” J. Micros. **217**, 93-108 (2005).